doi:10.1093/brain/aww298 BRAIN 2017: 140; 399–413 | 399

BRAIN
A JOURNAL OF NEUROLOGY

Myelin phagocytosis by astrocytes after myelin damage promotes lesion pathology

Gerald Ponath,[1] Sriram Ramanan,[1] Mayyan Mubarak,[1] William Housley,[1] Seunghoon Lee,[2] F. Rezan Sahinkaya,[3] Alexander Vortmeyer,[4] Cedric S. Raine[5] and David Pitt[1]

Astrocytes are key players in the pathology of multiple sclerosis and can assume beneficial and detrimental roles during lesion development. The triggers and timing of the different astroglial responses in acute lesions remain unclear. Astrocytes in acute multiple sclerosis lesions have been shown previously to contain myelin debris, although its significance has not been examined. We hypothesized that myelin phagocytosis by astrocytes is an early event during lesion formation and leads to astroglial immune responses. We examined multiple sclerosis lesions and other central nervous system pathologies with prominent myelin injury, namely, progressive multifocal leukoencephalopathy, metachromatic leukodystrophy and subacute infarct. In all conditions, we found that myelin debris was present in most astrocytes at sites of acute myelin breakdown, indicating that astroglial myelin phagocytosis is an early and prominent feature. Functionally, myelin debris was taken up by astrocytes through receptor-mediated endocytosis and resulted in astroglial NF-κB activation and secretion of chemokines. These *in vitro* results in rats were validated in human disease where myelin-positive hypertrophic astrocytes showed increased nuclear localization of NF-κB and elevated chemokine expression compared to myelin-negative, reactive astrocytes. Thus, our data suggest that myelin uptake is an early response of astrocytes in diseases with prominent myelin injury that results in recruitment of immune cells. This first line response of astrocytes to myelin injury may exert beneficial or detrimental effects on the lesion pathology, depending on the inflammatory context. Modulating this response might be of therapeutic relevance in multiple sclerosis and other demyelinating conditions.

1 Yale University, School of Medicine, Department of Neurology, 300 George St, New Haven, CT 06511, USA
2 Yale University, School of Medicine, Department of Ophthalmology and Visual Science, 300 George St, New Haven, CT 06511, USA
3 The Ohio State University College of Medicine, Department of Neuroscience, 670 Biomedical Research Tower, Columbus, OH, 43210, USA
4 Yale University, School of Medicine, Department of Pathology, 310 Cedar Street New Haven, CT 06520-8023, USA
5 Albert Einstein College of Medicine, Department of Pathology (Neuropathology), 1300 Morris Park Avenue, Bronx, NY 10461, USA

Correspondence to: Gerald Ponath,
Yale University, School of Medicine, Department of Neurology,
300 George St, Room 353,
New Haven, CT 06511, USA
E-mail: gerald.ponath@yale.edu

Keywords: astrocyte; multiple sclerosis and neuroinflammation; demyelination; neuroimmunology; T-lymphocytes

Abbreviations: iNOS = inducible nitric oxide synthase; LFB = Luxol Fast Blue; MAP = mitogen-activated protein

Received March 1, 2016. Revised October 14, 2016. Accepted October 17, 2016. Advance Access publication December 31, 2016

Introduction

The prototypical inflammatory demyelinating disease of the CNS is multiple sclerosis, a disease driven by an autoimmune response to self-antigens in genetically predisposed individuals (Nylander and Hafler, 2012). The pathological hallmark of multiple sclerosis is demyelinating lesions infiltrated by T lymphocytes and macrophages (Lassmann *et al.*, 2007), yet the early events that lead to immune infiltration and subsequent inflammatory demyelination are still not completely understood.

Contrary to previously held beliefs, astrocytes do not merely respond to demyelination by forming a glial scar in late postinflammatory stages, but are early and highly active players during lesion development (Brosnan and Raine, 2013). In acute lesions, astrocytes assume a hypertrophic morphology characterized by massive enlargement, reduced process density, multiple nuclei. Due to their presence within acute lesions and at the active margin of subacute lesions, astroglial hypertrophy is considered one of the earliest events in the demyelinating process (Brosnan and Raine, 2013). This notion is further supported by the presence of reactive astrocytes and axonal damage before significant numbers of immune cells infiltrate the parenchyma in experimental autoimmune encephalomyelitis (EAE), an animal model of inflammatory demyelination (D'Amelio *et al.*, 1990; Wang *et al.*, 2005; Pham *et al.*, 2009). It is therefore unclear whether early astroglial activation in nascent multiple sclerosis lesions is initiated by the inflammatory environment generated by infiltrating immune cells or by other triggers (Croitoru-Lamoury *et al.*, 2003).

Previous work has shown that hypertrophic astrocytes in active multiple sclerosis lesions contain myelin fragments, suggesting that myelin is phagocytosed by astrocytes (Lee *et al.*, 1990; Morcos *et al.*, 2003). We hypothesized that phagocytosing of damaged myelin by hypertrophic astrocytes is an early response that impacts on subsequent lesion development. Moreover, as hypertrophic astrocytes have been described in active zones of other CNS pathologies associated with prominent myelin damage (Greenfield *et al.*, 2008), myelin uptake by astrocytes might be a universal response not restricted to multiple sclerosis. We addressed these questions by examining the prevalence and distribution of myelin debris-containing astrocytes in autopsy tissue of multiple sclerosis, progressive multifocal leukoencephalopathy, cerebral infarct and metachromatic leukodystrophy. We also examined the functional consequences of myelin uptake in primary astrocyte cultures and in autopsy tissue. Our results provide compelling evidence that uptake of myelin debris by astrocytes is a common, if not consistent feature associated with myelin breakdown and an important mechanism for immune cell recruitment to the lesion site.

Material and methods

Tissue samples

Human CNS tissue was obtained at autopsy according to Institutional Review Board-approved protocols. CNS tissue was obtained from nine subjects with multiple sclerosis, one subject with progressive multifocal leukoencephalopathy, one subject with metachromatic leukodystrophy and five subjects with subacute ischaemic infarct (Supplementary Table 1). Post-mortem intervals ranged between 3 and 32 h. Brain tissue was fixed with 10% formalin for 2 to 4 weeks and embedded in paraffin.

The multiple sclerosis patient cohort consisted of one acute case who was biopsied (Patient MS1), five cases of relapsing/remitting multiple sclerosis, two cases of secondary progressive multiple sclerosis and one case of asymptomatic multiple sclerosis that was incidentally discovered at autopsy (Patient MS9). Patient MS1 was a 62-year-old female with one month disease duration. Patient MS2 was a 50-year-old female with 13 years disease duration who died of cardiopulmonary arrest. Patient MS3 was a 31-year-old female with 8 years disease duration who died of respiratory failure. Patient MS4 was a 32-year-old male with 10 years disease duration who died of pneumonia. Patient MS5 was a 50-year-old female with 10 years disease duration who died of respiratory failure. Patient MS6 was a 39-year-old male with >15 years disease duration who died of haemorrhagic bronchopneumonia. Patient MS7 was a 65-year-old male with 30 years disease duration who died of chronic cystitis. Patient MS8 was a 58-year-old male with 27 years disease duration with unknown cause of death; and Patient MS9 was a 68-year-old male with unknown disease duration who died of cardiac arrhythmia. The expanded disability status scale (EDSS) scores of the patients at the time of their deaths are not known. We examined a total of 25 white matter lesions of which 20 lesions were early or chronic active and five lesions were chronic silent.

The patient with progressive multifocal leukoencephalopathy (Patient PML1) was a 55-year-old male with multiple sclerosis of 6 years disease duration who subsequently developed and died of progressive multifocal leukoencephalopathy after receiving treatment with natalizumab for 4 years. The patient with metachromatic leukodystrophy (Patient MLD1) was a 3-year-old male with metachromatic leukodystrophy who died in status epilepticus.

Infarct patient 1 (Patient CVA1) was 68-year-old male with a 20-day-old infarct of the entire right middle cerebral artery territory who died of brainstem compression. Infarct patient 2 (Patient CVA2) was a 79-year-old male with a 2-month-old infarct in the left middle cerebral artery territory involving the superior and middle temporal gyri, who died of sepsis. Infarct patient 3 (Patient CVA3) was 69-year-old

male with multiple 2-week-old white matter watershed infarcts, who died of acute myocardial infarction. Infarct patient 4 (Patient CVA4) was 67-year-old female with an 18-day-old infarct of the entire left middle cerebral artery territory who died of metastatic pancreatic adenocarcinoma. Infarct patient 5 (Patient CVA5) was a 48-year-old male with a subacute infarct of the right frontal lobe (middle cerebral artery territory) who died of sepsis.

Immunohistochemistry and histochemistry

Formalin-fixed, paraffin-embedded (FFPE) sections were cut at 5 -µm thickness. After quenching with 0.03% hydrogen peroxide and blocking with normal serum, sections were incubated with primary antibodies overnight (Supplementary Table 2), processed with the appropriate biotinylated secondary antibody and avidin/biotin staining kit with diaminobenzidene and VIP as chromogens (Vector ABC Elite Kit, DAB Kit and VIP Kit, Vector Laboratories), and counterstained with haematoxylin (Pitt *et al.*, 2003). For fluorescence, sections were incubated with fluorescent-labelled secondary antibodies and subsequently treated with 0.7% Sudan Black in ethanol and $CuSO_4$ to quench autofluorescence. Sections were counterstained with DAPI and mounted with VectaShield mounting medium (VectaShield Kit, Vector Laboratories). Adequate controls using isotype control antibodies were performed with each primary antibody.

For staining of myelin proteins with Luxol Fast Blue (LFB), FFPE sections were incubated overnight with LFB at 56°C and subsequently washed in 95% ethanol and dH_2O. The colour was discriminated in Li_2CO_3 solution and differentiated in 70% ethanol. In formalin-fixed, OCT-embedded sections, i.e. in tissue in which lipids are not extracted through deparaffinization (Patient MS9), myelin lipids were detected with Sudan Red 5B (Oil Red O), which stains neutral lipids. Sections were incubated with Oil Red O for 10 min, washed with tap water, counterstained with haematoxylin and cover-slipped with aqueous mounting medium without dehydration (Mehlem *et al.*, 2013). Both stains were combined with immunohistochemical labelling against GFAP and CD68.

Brightfield images were acquired with a Leica DM5000 B microscope using a Leica colour camera DFC310 Fx and the Leica Application Suite (version 4.2.0) imaging software. Fluorescent images were taken with an UltraVIEW VoX (Perkin Elmer) spinning disc confocal Nikon Ti-E Eclipse microscope. Image acquisition, visualization and quantification were performed using the Volocity 6.3 software (Improvision). Images were processed with the ImageJ software (Schneider *et al.*, 2012).

Nuclear localization of NF-κB and chemokine expression levels of CCL3, CCL5, CCL20 and CXCL10 as well as inducible nitric oxide synthase (iNOS) were quantified by densitometric analysis of fluorescent immunoreactivity of various cell types. Acquisition and analysis were performed in a double-blinded manner. Statistical analysis was based on expression levels of at least 20 cells per cell type per case in four multiple sclerosis cases, two cerebral infarct cases and one case of progressive multifocal leukoencephalopathy.

Multiple sclerosis lesion classification

For basic characterization, sections were immunolabelled for myelin basic protein (MBP; myelin), glial fibrillary acidic protein (GFAP; astrocytes), and CD68 (macrophages, microglia). Multiple sclerosis lesions were categorized into early active, chronic active and chronic silent lesions. Early active lesions were characterized by hypercellularity, oedema, lymphocytic and intense macrophage infiltration with ongoing demyelination and astroglial hypertrophy. Chronic active lesions were characterized by central chronic demyelination and astrogliosis with active demyelination at the lesion margin. Chronic silent lesions consisted of areas of demyelination, astrogliosis and absence of inflammation (Werner *et al.*, 2001).

Myelin purification

Myelin was purified as described by Norton and Poduslo (1973). In brief, adult male Sprague-Dawley rat spinal cords were homogenized in 0.32 M sucrose using a Dounce homogenizer. Myelin was recovered by three successive sucrose gradient centrifugation steps and washed extensively in Tris·Cl buffer, pH 7.4. The pellet was resuspended in 0.32 M sucrose, layered over 0.85 M sucrose and subjected to centrifugation at 75 000 *g* for 30 min. Myelin was recovered and suspended in phosphate-buffered saline (PBS) pH 7.4. Protein concentration of the preparation was analysed with a BCA-Kit (Pierce), according to the manufacturer's instructions.

Cell culture

Cultures of glial cells were prepared according to the method of McCarthy and de Vellis (1980). Briefly, cerebral cortex from postnatal Day 1 Sprague-Dawley rat pups was isolated, minced, and digested for 30 min at 37°C in Hanks' balanced salt solution (HBSS) containing 0.25% trypsin (Life Technologies). Cells from each rat were plated in separate 75 cm^2 tissue culture flasks coated with 10 µg/ml of poly-L-lysine. Cultures were maintained in Dulbecco's modified Eagle medium (DMEM) with 10% foetal bovine serum (FBS) and penicillin/streptomycin for 10 days. Flasks were agitated by rotation (180 rpm) for 30 min at 37°C to detach and collect microglia. Finally,

astrocytes were collected after Accutase® treatment and were further purified with astrocyte-specific glutamate transporter anti-glutamate aspartate transporter (GLAST) antibodies linked to magnetic microbeads (Miltenyi Biotec) according to the manufacturer's instructions. Astrocytes were plated in tissue culture dishes coated with 10 µg/ml of poly-L-lysine and cultured in DMEM with 10% FBS and penicillin/streptomycin. To assess purity of the primary cultures, immunostaining was performed using cell-type-specific antibodies targeting isolectin B4 (microglia) and GFAP (astrocytes).

Myelin uptake assays

Purified myelin was labelled with Oregon Green® 488 Dye (Life Technologies) according to the manufacturer's instructions. Myelin was incubated with cells for various durations ranging from 30 min to 72 h at 37°C. For quantification of myelin uptake by astrocytes, we washed astrocytes three times with PBS to release surface-associated myelin. We omitted pronase treatment of astrocytes suggested in previous protocols (Gaultier *et al.*, 2009) as the washing step sufficiently removed myelin debris from astroglial cell surfaces, as demonstrated with confocal *z*-stack images of astrocytes at various time points of myelin exposure. Quantitative assessment of myelin uptake was performed with a fluorescence plate reader (Infinite M1000 Pro, Tecan). Myelin uptake was assessed qualitatively up to 24 h after incubation with fluorescence microscopy using a spinning disc confocal Nikon Ti-E Eclipse microscope. Images were processed using the ImageJ software (Schneider *et al.*, 2012). In some studies, LysoTracker® or CellROX® (Life Technologies) was added 30 min prior to fixation.

Immunocytochemistry

After treatment, astrocyte cultures were washed with PBS, fixed in 4% paraformaldehyde/PBS for 20 min, washed, blocked and permeabilized for 1 h in 10% goat serum, 1% bovine serum albumin, and 0.01% Triton™ X-100 at room temperature. Cultures were incubated in blocking buffer with primary antibody (2 µg/ml) overnight at 4°C and subsequently with fluorescent-labelled secondary antibody (1 µg/ml, Life Technologies) for 2 h at room temperature. Primary antibodies used to identify astrocytes and cell organelles are listed in Supplementary Table 2. Cell nuclei were visualized with Hoechst® dye 33 342 (1:100 000 in PBS for 5 min). Cultures were washed three times and mounted in ProLong® Gold antifade reagent (Life Technologies).

Flow cytometry, ELISPOT and immunoblotting

Astrocytes were incubated with purified myelin ranging from 15 min to 2 h and dissociated with Accutase® (Life Technologies) for flow cytometry analysis following published procedures (Housley *et al.*, 2011). Briefly, cells were stained for 15 min at room temperature with fluorescent-labelled primary antibodies, washed, and analysed on either a FACSCalibur™ or a LSRII flow cytometer (BD Biosciences). Cytokine release was quantified using an enzyme-linked immunospot (ELISPOT) array (RAT Cytokine Proteome Profiler, R&D Systems). Supernatants from astrocyte cultures exposed previously to purified myelin for 24–48 h were collected and centrifuged (3000 rpm for 10 min) before analysis. All assays were performed according to the manufacturer's instructions. Immunoblotting was performed by published procedures (Ponath *et al.*, 2007). Briefly, following stimulation with purified myelin, cultured astrocytes were lysed for whole protein fractions in the presence of a proteinase inhibitor cocktail. Sodium dodecyl sulphate-polyacrylamide gel electrophoresis (SDS-PAGE) was performed using NuPAGE® 10% Bis–Tris gels (Life Technologies) with MOPS running buffer and subsequent transfer of blots on nitrocellulose membranes. Primary antibodies used for immunodetection are listed in Supplementary Table 2. After incubation with secondary antibodies, proteins were visualized with an enhanced chemiluminescence using an ImageQuant™ LAS 4000 camera (GE Healthcare).

Extraction of total RNA and polymerase chain reaction array

For expression profiling of 84 key genes involved in autoimmune and inflammatory immune responses, we used the Rat Inflammatory Response & Autoimmunity RT^2 Profiler PCR Array (Qiagen), according to the manufacturer's instructions. Astrocytes were incubated with 4 ng/ml purified myelin for 4 h before total RNAs were extracted (miRNeasy® Mini Kit; Qiagen). The PCR array was run on a StepOne™ Real-time PCR system (Life Technologies). Data were analysed using web-based software (http://pcrdataanalysis.sabiosciences.com /pcr/arrayanalysis.php), based on the $\Delta\Delta C_T$ method with normalization of the raw data to five housekeeping genes.

Statistical analysis

Results were expressed as standard deviation (SD) of the mean. Data were analysed by one-way ANOVA followed by the Tukey-Kramer multiple comparison test.

Study approval

Human CNS tissue was obtained according to Institutional Review Board-approved protocols.

Yale's Institutional Animal Care and Use Committee (IACUC) granted approval for the use of animals in this project (#2013-11543). Yale University has an approved Animal Welfare Assurance (#A3230-01) on file with the

NIH Office for Protection from Research Risks. The Assurance was approved May 12, 2011.

Results

Astroglia containing myelin debris are present in various demyelinating CNS diseases

To investigate the prevalence of astrocytes with myelin debris in diseases with prominent myelin injury, we examined autopsy tissue from patients with multiple sclerosis, progressive multifocal leukoencephalopathy, metachromatic leukodystrophy and subacute ischaemic infarct. The majority of astrocytes in acute multiple sclerosis lesions (biopsy, Fig. 1A–D) and at the edges of ongoing demyelination in chronic active lesions (Fig. 1E–N), had a hypertrophic morphology characterized by a ballooned appearance with short, thickened processes and enlarged, occasionally multiple nuclei. These astrocytes contained LFB-positive inclusions and Oil Red O-positive lipid droplets, suggesting presence of myelin debris (Fig. 1C, G and H). Astrocytes in gliotic, inactive lesion centres showed small nuclei and small amounts of delicate fibrillary cytoplasm (Fig. 1B, C, E, F, I and L) and were uniformly LFB/Oil Red O-negative (Fig. 1F and L). Confocal microscopy confirmed that hypertrophic astrocytes contained intracellular MBP- and PLP1-positive puncta (Fig. 1D, J and K), whereas fibrous astrocytes in normal-appearing white matter or gliotic lesions were immunonegative for myelin proteins. In addition, PLP-positive puncta within astrocytes were located within lysosomal ring structures visualized with the lysosomal marker, LAMP1 (Fig. 1D and K). This finding further establishes the intracellular localization of myelin debris and its degradation through the lysosomal pathway. Moreover, myelin debris co-localized with the cell surface scavenger receptor low density lipoprotein receptor-related protein 1 (LRP1; Fig. 1M), indicating that myelin uptake is mediated by LRP1. The number of myelin-containing, hypertrophic astrocytes was approximately one-third of myelin-laden macrophages; however, the amount of myelin debris within astrocytes was only 5% of that in macrophages (Supplementary Fig. 1), suggesting that the bulk of myelin is removed by macrophages. In addition, we found that myelin-containing hypertrophic astrocytes were present to a lesser degree in the perimeter of active lesions, i.e. in normal-appearing white matter, which contains scattered activated microglia but not myelin-laden phagocytes (Supplementary Fig. 2).

We also studied progressive multifocal encephalopathy, a demyelinating disease caused by JC virus (Boster *et al.*, 2013). Acute progressive multifocal leukoencephalopathy lesions and occasionally adjacent brain tissue displayed numerous hypertrophic astrocytes with enlarged, bizarrely shaped nuclei, a characteristic feature of progressive multifocal leukoencephalopathy (Fig. 2A–C). The majority of hypertrophic astrocytes within the demyelinating lesion but not in adjacent white matter contained small LFB-positive inclusions (Fig. 2D and E). Confocal microscopy on fluorescent-labelled sections confirmed the presence of MBP in lesional hypertrophic astrocytes but not in astrocytes in normal-appearing white matter (Fig. 2F and G). In progressive multifocal leukoencephalopathy, we observed a population of myelin-negative hypertrophic astrocytes that was not present in multiple sclerosis or cerebral infarcts. This is unsurprising as astroglial hypertrophy is a hallmark of progressive multifocal leukoencephalopathy presumably caused by JC virus proliferating within astrocytes.

Furthermore, we examined CNS tissue from a case of metachromatic leukodystrophy. Metachromatic leukodystrophy is a U-fibre sparing leukodystrophy in which sulphatide and lysosulphatide accumulate due to arylsulphatase A deficiency in lysosomes (Gieselmann and Krageloh-Mann, 2010). Myelin loss along with axonal destruction, the pathological hallmark of metachromatic leukodystrophy is thought to be caused by critical sulphatide levels in oligodendrocytes and Schwann cells. Immunolabelling with MBP and CD68 showed a gradient of demyelination from near-intact U-fibres to myelin-depleted white matter with diffuse macrophage infiltration (Fig. 2H–K). As with multiple sclerosis and progressive multifocal leukoencephalopathy, hypertrophic astrocytes were present in zones of ongoing myelin destruction and contained PLP-positive myelin debris (Fig. 2M and P). In contrast, myelin-depleted white matter in metachromatic leukodystrophy contained a dense gliotic mesh with infrequent and small astrocytic cell bodies from which myelin debris was absent (Fig. 2N and Q). Reactive astrocytes in subcortical areas with preserved myelin were also PLP-negative (Fig. 2L and O).

Finally, we examined five cases of subacute cerebral infarcts ranging from 2 to 9 weeks in age. In all cases, the necrotic core of the infarct was surrounded by a myelin-depleted, reactive zone with hypertrophic (gemistocytic) astrocytes (Fig. 3A–E and G). In areas of acute myelin breakdown within the reactive zone, hypertrophic astrocytes but not activated astrocytes in the bordering myelinated white matter contained PLP1-positive myelin debris (Fig. 3F, G, I and J). In the necrotic core, no astrocytes were present and myelin debris was found in infiltrating macrophages (Fig. 3H and K). As with multiple sclerosis, the ratio of myelin-containing astrocytes to macrophages indicates that the majority of damaged myelin is cleared by macrophages (Supplementary Fig. 1).

In summary, in all CNS diseases that we examined, hypertrophic astrocytes were the predominant astroglial phenotype in areas of acute myelin breakdown of which the vast majority contained myelin debris. Reactive astrocytes in normal appearing white matter and fibrotic astrocytes within gliotic scars were uniformly myelin-negative. Moreover, intracellular myelin debris was associated with LRP1 and with LAMP1 suggesting a receptor-based mechanism for astroglial myelin uptake and lysosomal degradation.

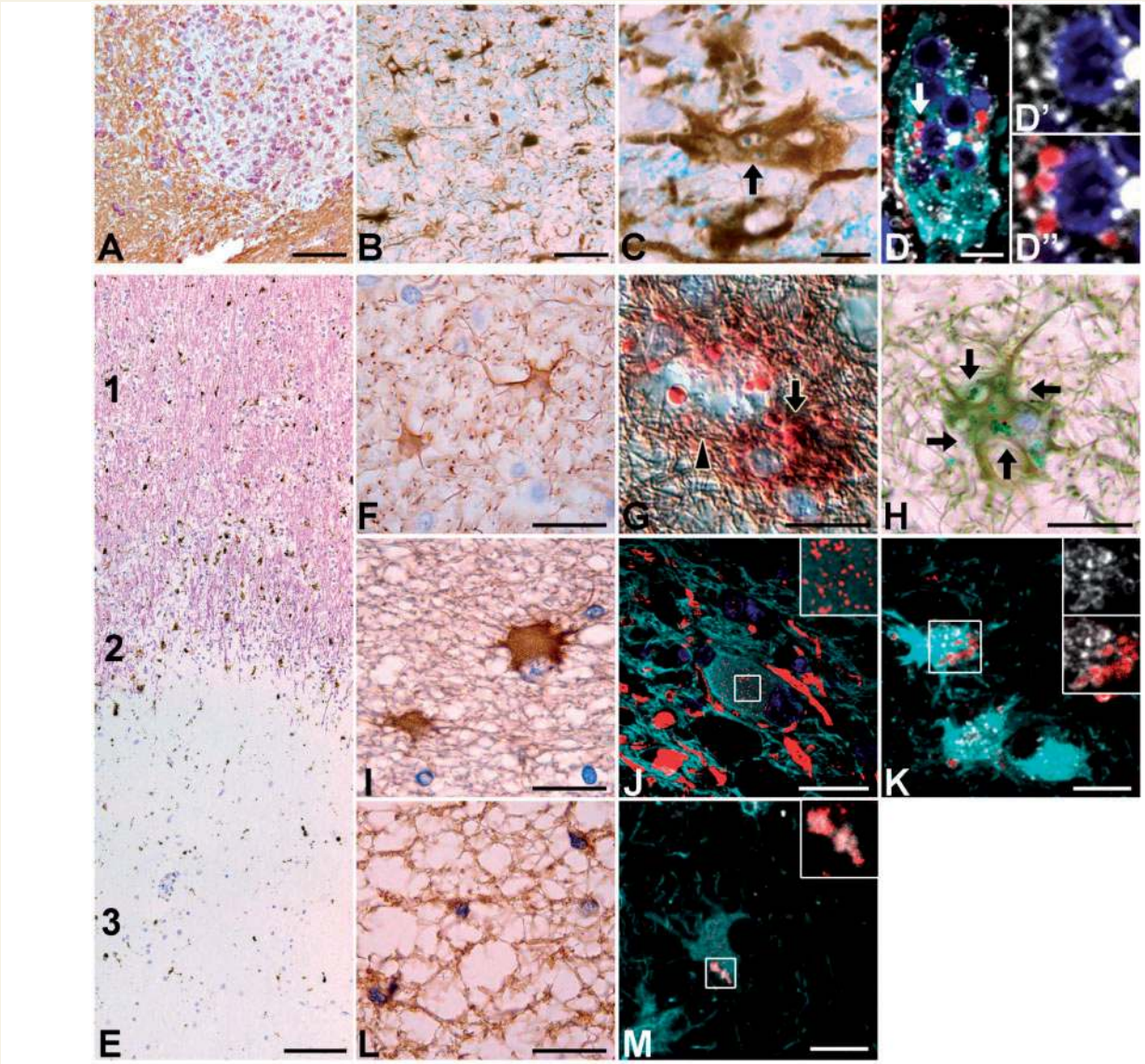

Figure 1 Hypertrophic astrocytes in active white matter multiple sclerosis lesions contain myelin debris. (**A**) Low magnification of an acute multiple sclerosis lesion (biopsy) filled with foamy macrophages (MBP, brown; CD68, purple). (**B**) Reactive astrocytes (GFAP, brown) within the acute lesion are hypertrophic with rarefied, thickened processes. (**C**) Higher magnification shows LFB-positive inclusions within astroglia (arrow). (**D**) Confocal microscopy confirms the presence of the myelin protein, PLP1 (red) in an astrocyte. (**D'** and **D**") Higher magnification shows PLP-positive puncta within ring-like structures labelling positive for the lysosomal marker LAMP1 (LAMP1, white; GFAP, cyan; nuclei, blue). (**E**) Low magnification of the edge of a chronic active lesion with macrophage infiltrates at the lesion rim and in the adjacent white matter (CD68, brown; MBP, purple). (**F**) GFAP staining shows reactive astrocytes in adjacent white matter, (**I**) reactive hypertrophic astrocytes at the lesion edge and (**L**) small, chronic-reactive astrocytes in the gliotic lesion centre. (**G**) As in acute lesions, hypertrophic astrocytes (GFAP, brown) at the lesion edge contain neutral lipid droplets, visualized with Oil Red O, and (**H**) LFB-positive inclusions, both indicative of myelin debris (arrows). Oil Red O-positive droplets are also seen in a macrophage next to the astrocyte (arrowhead). (**J**) Confocal microscopy of a ballooned astrocyte double-labelled for GFAP (cyan) and intracellular accumulation of MBP-positive myelin fragments (red; see inset). (**K**) PLP-positive myelin debris (red) within astrocytes (GFAP, cyan) is present in lysosomes (LAMP1, white; see inset) and (**M**) co-localizes with the scavenger receptor LRP1 (white; inset). Scale bars = 100 μm in **A**, **B**, **E**; 25 μm in **C**, **D**, **F**, **G**, **H**, **I**, **L**; 20 μm in **J**; and 10 μm in **K** and **M**.

Astrocytes take up myelin debris in a concentration-dependent manner

We modelled the functional impact of myelin uptake on astrocytes by exposing cultured primary cortical rat astrocytes to purified myelin fragments. Differentiated astrocytes (*in vitro* Day 14) were purified with GLAST antibodies linked to magnetic microbeads (>98% purity, Supplementary Fig. 3) and cultured as a confluent monolayer and incubated with various concentrations of fluorescent-labelled myelin purified from rat spinal cord. Within 24 h, all myelin was cleared from the supernatant and was

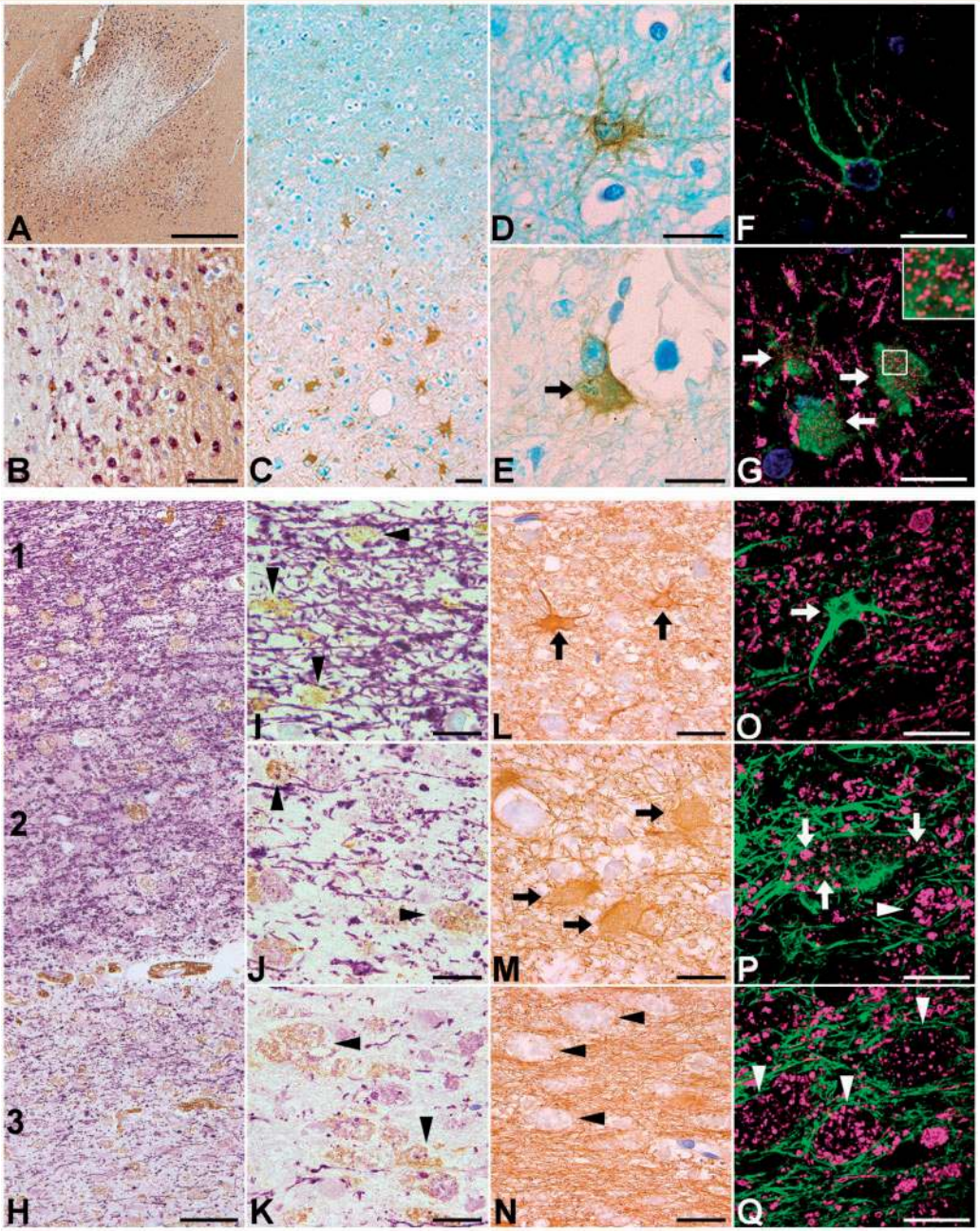

Figure 2 Myelin debris-positive hypertrophic astroglia in progressive multifocal leukoencephalopathy lesions and metachromatic leukodystrophy. (**A**) Low magnification image of a subacute progressive multifocal leukoencephalopathy lesion with infiltrating microglia/macrophages at the lesion rim and the adjacent white matter (MBP, brown; CD68, purple). (**B**) Higher magnification shows foamy macrophages at the lesion edge. (**C**) Numerous hypertrophic astrocytes are present within the lesion and the lesion edge but not in adjacent white matter (GFAP, brown; myelin, LFB). (**D** and **E**) Astrocyte in myelinated white matter remote from the lesion without myelin inclusions. In contrast, a perivascular astrocyte at the lesion rim contains LFB-positive debris (arrow). (**F** and **G**) Confocal microscopy confirms the presence of MBP (magenta) in GFAP-labelled astrocytes (green) at the lesion rim (**G**; white arrows, inset) but not in adjacent white matter (**F**). (**H**) Low magnification of metachromatic leukodystrophy white matter shows areas of subcortical U-fibres with apparently intact myelin (**H1**; detail in **I**), of ongoing myelin damage (**H2**; detail in **J**) and of myelin-depleted white matter (**H3**; detail in **K**); double labelling for myelin and macrophages (MBP, purple; CD68, brown). (**I–K**) Numerous macrophages are scattered throughout the intact and demyelinated white matter (arrowheads). (**L** and **O**) Activated astrocytes in subcortical myelinated white matter are highly immunoreactive for GFAP (brown) but do not contain PLP-positive debris (GFAP, green; PLP, magenta) (arrows). (**M** and **P**) The zone with ongoing myelin damage is filled with hypertrophic astrocytes (GFAP, brown) that contain PLP-positive myelin fragments (arrows), visualized with confocal microscopy (GFAP, green; PLP, magenta). (**N** and **Q**) Gliotic fibres with occasional astroglial cell bodies predominate in myelin-damaged white matter (GFAP, brown). PLP-positive debris (magenta) is present in macrophages (arrowheads) that are interspersed among the GFAP-positive fibrous mesh (green). Scale bars = 1000 μm in **A**; 100 μm in **B**, **C** and **H**; 25 μm in **D**, **E** and **I–N**; and 20 μm in **F**, **G**, **O–Q**.

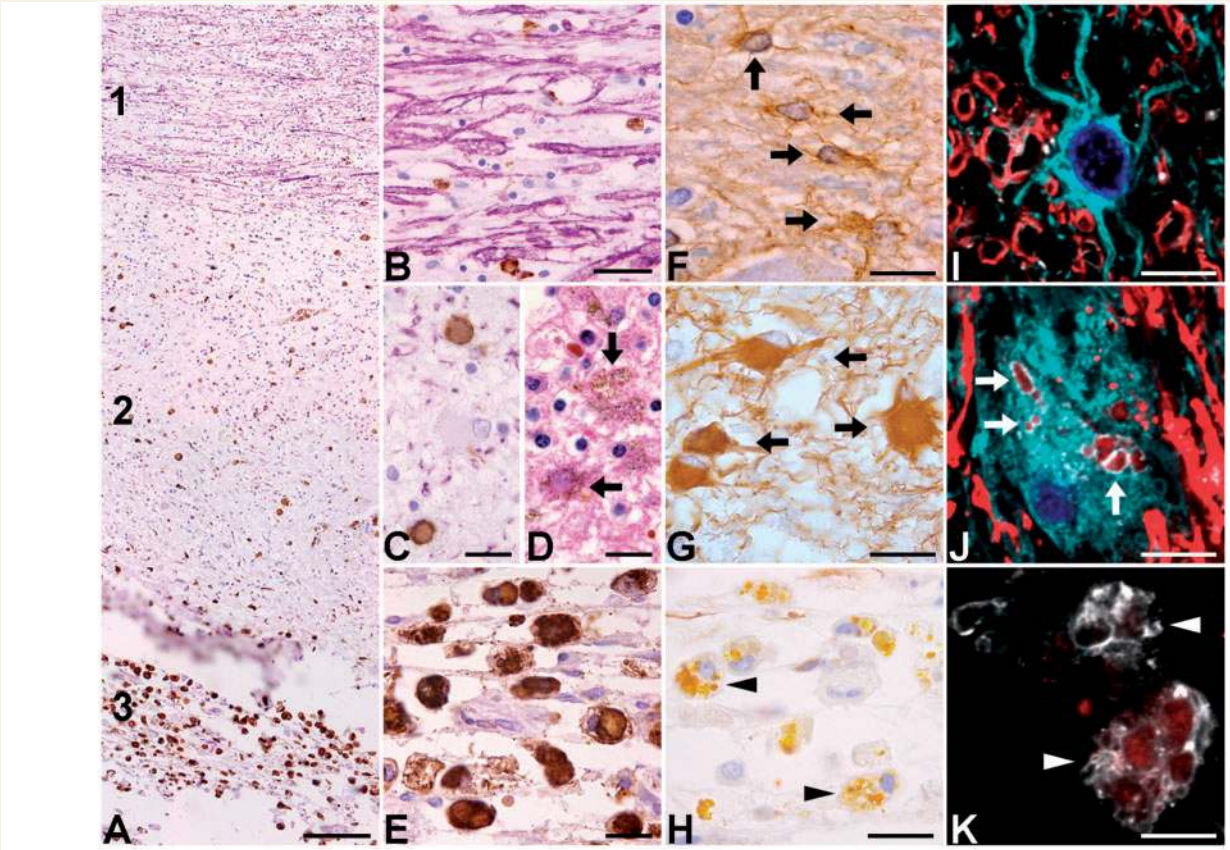

Figure 3 Myelin debris-positive hypertrophic astrocytes in the reactive zone of a subacute infarct. (**A**) Overview image of a subacute infarct double-labelled for MBP (purple) and CD68 (brown). Myelin is present at the infarct border (**A1**, detail in **B**). The reactive zone surrounding the infarct centre shows loss of myelin and contains infiltrating macrophages (**A2**, detail in **C**). The necrotic core is filled with foamy $CD68^+$ macrophages (**A3**, detail in **E**). (**D**) Two astrocytes in the reactive zone contain hemosiderin (arrows; haematoxylin/eosin). **(F)** Reactive astrocytes in myelinated white matter at the lesion border. **(G)** Hypertrophic (gemistocytic) astrocytes in the reactive zone (arrows). **(H)** Astrocytes are absent from the infarct core. Arrowheads indicate hemosiderin-laden macrophages. (**I**) Confocal microscopy shows an activated astrocyte in intact white matter without myelin debris. (**J**) PLP1-positive myelin debris in lysosomes of a proliferating hypertrophic astrocyte within the reactive zone (arrows). (**K**) PLP1-positive debris is present in lysosomes of macrophages at the infarct core. (PLP1, red; LAMP1, white; GFAP, cyan). Scale bars = 100 μm in **A**; 25 μm in **B–H**; and 10 μm in **I–K**.

present in the majority of astrocytes (Fig. 4A). Flow cytometry confirmed that >98% of astrocytes contained fluorescent myelin debris as early as 45 min after myelin exposure. Intracellular localization of myelin was visualized by orthogonal views of *z*-stack images acquired by confocal microscopy (Fig. 4B).

Myelin uptake in isolated astrocyte cultures was concentration-dependent and linear within the first hour at a concentration range of 0.125 to 2 μg/ml (Fig. 4C). Myelin uptake by astrocytes was also observed when co-cultured with microglia, albeit at a lower level, since microglia competed for myelin debris and phagocytosed with higher efficiency. In addition, myelin uptake was independent of astroglial density and maturation stage (*in vitro* Days 14–40). Astroglial activation with TNFα and IFNγ increased myelin uptake by 25% [one-way ANOVA, $F(3,8) = 9.51$, $P = 0.005$; Tukey–Kramer test, $P < 0.05$], while incubation with lipopolysaccharide (LPS; all 10 ng/ml for 24 h) did not change myelin uptake compared to resting astrocytes.

Myelin is taken up by LRP1-mediated endocytosis and is degraded in lysosomes

To examine uptake mechanisms and intracellular trafficking of myelin debris, we immunolabelled cultured astrocytes for the cell surface receptor LRP1 and with markers of the endosomal lysosomal pathway. Fluorescent-labelled myelin fragments within astrocytes co-localized with LRP1 after 30 min, with the endosomal marker early endosome antigen-1 (EEA1) after 60 min and with the lysosomal markers, Lysotracker Red™ and CellROX™ at 120 min (Fig. 4E–H). Time-lapse images demonstrated lysosomal degradation of myelin debris over time indicated by loss of green fluorescence within lysosomes (Fig. 4H). To confirm that

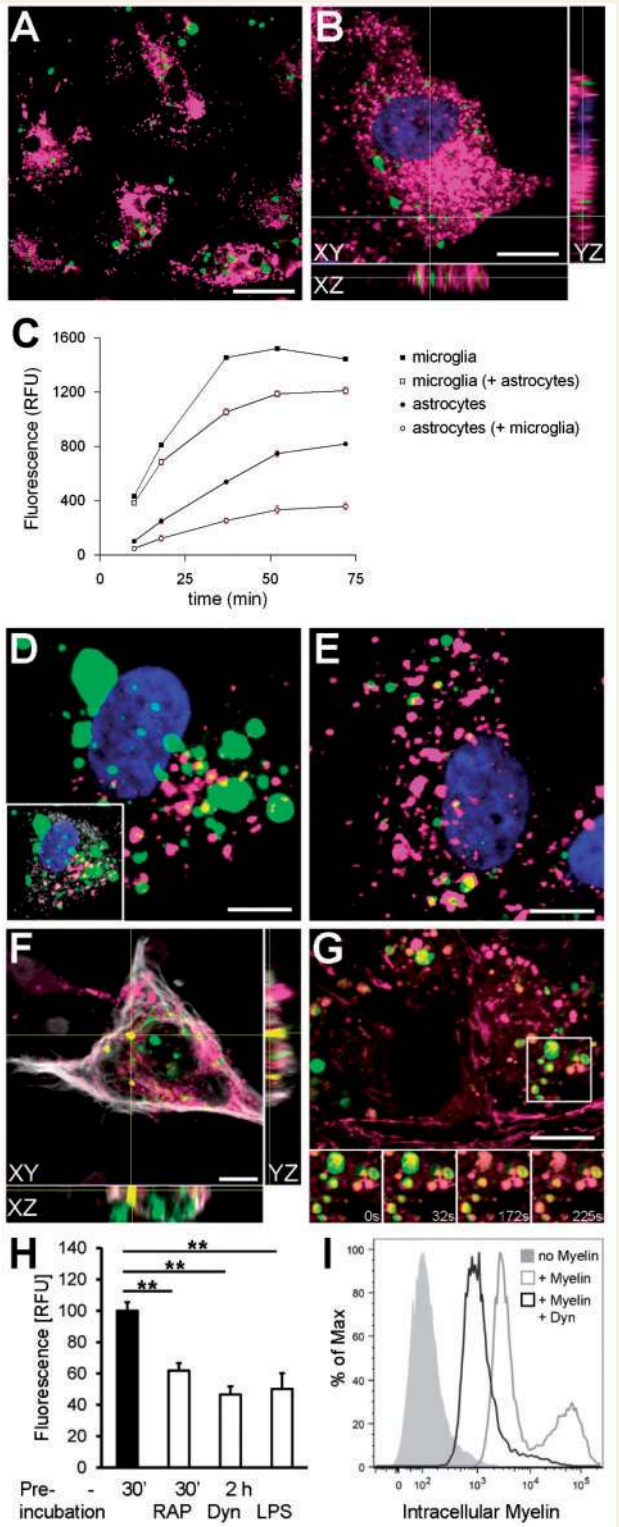

Figure 4 Kinetics and mechanism of myelin uptake in cultured astrocytes. (**A**) Primary rat cortical astrocytes (*in vitro* Day 14) containing fluorescent-labelled purified myelin after 24 h of myelin exposure (1 μg/ml) (S100B, magenta; myelin, green). (**B**) Intracellular localization of fluorescent myelin debris demonstrated with orthogonal views of confocal z-stack images of a representative astrocyte (S100B, magenta; myelin, green). (**C**) Accumulation of fluorescence in isolated cultured astrocytes and microglia cells after 30 min of exposure to various concentrations of fluorescent-labelled myelin (0.0625 μg/ml to 2 μg/ml). In co-cultures, astrocytes and microglia were separated with magnetic beads before quantification. Graphs show mean ± SD from three independent experiments of the quantification of Oregon Green® 488-labelled myelin. (**D**) Cultured astrocytes containing myelin fragments after 30 min of myelin exposure. Myelin particles partially co-localize with the cell surface receptor LRP1 (myelin, green; LRP1, magenta; H 33342, blue; ALDH1L1, grey in inset). (**E**) Partial co-localization of intracellular myelin debris with the early endosomal marker, EEA1, in astrocyte exposed to myelin for 60 min (EEA1, magenta; myelin, green). (**F** and **G**), Intracellular myelin debris co-localized with lysosomes after 120 min of myelin exposure demonstrated with the lysosomal markers LysoTracker™ and CellROX (both magenta). (**G**; inset) Rapid degradation of myelin debris (green) in CellROX-positive lysosomes shown with time-lapse recording. (**H**) Myelin uptake in cultured astrocytes is reduced by the competitive LRP1 ligand RAP (5 μg/ml), the dynamin-dependent endocytosis blocker Dynasore (0.1 μM; 30 min preincubation) and by LPS (10 ng/ml, 2 h preincubation). Data represent the means ± SD from three independent experiments. **Means were significantly heterogeneous [one-way ANOVA, $F(3,9) = 70.55$, $P < 0.0001$] and significantly different from the control condition (Tukey–Kramer test, $P < 0.01$). (**I**) Flow cytometry analysis of astrocytes after 45 min incubation with myelin (2 μg/ml + DMSO 1:500). Cells were gated for GLAST$^+$ living cells. A representative graph from five independent experiments shows per cent of maximum fluorescence intensity of intracellular myelin. Pretreatment with Dynasore (0.1 μM in DMSO 1:500 for 30 min) resulted in 90% reduction of mean fluorescence intensity. DMSO (1:500) shows no effect of myelin uptake (data not shown). Scale bars = 30 μm in **A**; 15 μm in **B** and **E–H**.

myelin uptake by astroglia was a receptor-mediated, endocytotic process, we quantified myelin phagocytosis in astrocyte cultures preincubated with the competitive LRP1 antagonist, receptor associated protein (RAP; 5 μg/ml) and with Dynasore (0.1 μM, both 30 min), an inhibitor of dynamin-dependent endocytosis. Incubation of both RAP and Dynasore resulted in significantly reduced myelin endocytosis by astrocytes. Similarly, preincubation with LPS for 2 h resulted in reduced myelin uptake, consistent with LRP1-depleting effect of LPS from the cell surface (Fig. 4I) (Costales *et al.*, 2013). These results were confirmed by flow cytometry where pretreatment with Dynasore blocked myelin ingestion by >90% (Fig. 4J).

Myelin uptake induces astroglial activation

To elucidate the effect of myelin uptake on astrocyte function, we examined astroglial proliferation and activation markers. Astroglial proliferation following myelin endocytosis was measured through bromodeoxyuridine (BrdU)-incorporation and showed a 3-fold increase over untreated controls, compared to a 5-fold increase with TGF-β (10 ng/ml), a potent inducer of astroglial proliferation (Fig. 5A) (Yu *et al.*, 2014). In addition, GFAP was upregulated in astrocytes after 24 h of myelin exposure and

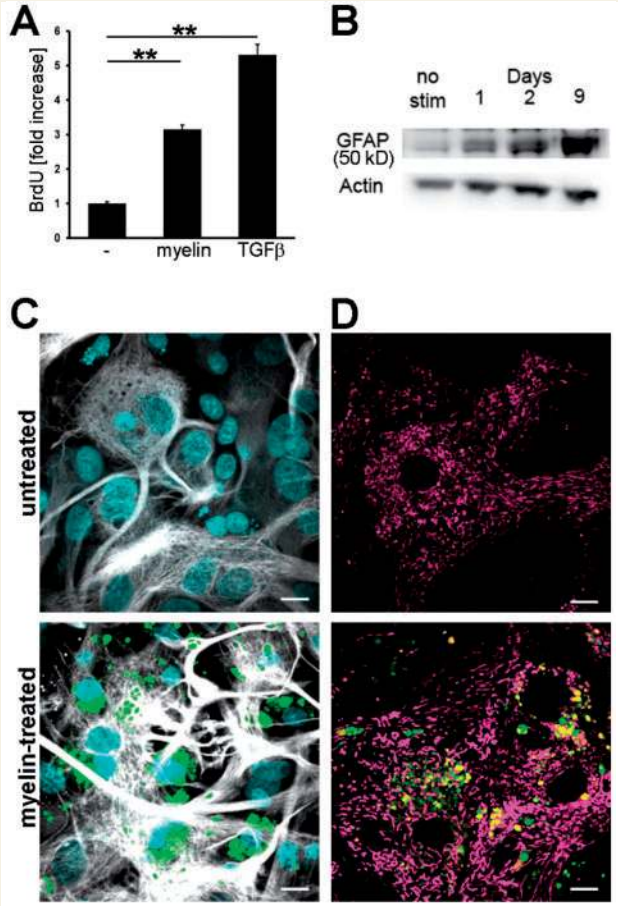

Figure 5 Myelin uptake induces astroglial activation and proliferation. (**A**) Increased astroglial proliferation after myelin uptake (1 μg/ml for 72 h) compared to TGFβ-induced proliferation (10 ng/ml), measured by BrdU-incorporation. Myelin concentration 1 μg/ml. Data represent the means ± SD from four independent experiments. **Means were significantly heterogeneous [one-way ANOVA, $F(2,21) = 21.41$, $P < 0.0001$] and significantly different from the control condition (Tukey–Kramer test, $P < 0.01$). (**B**) GFAP expression increases for at least 9 days after myelin stimulation (western blot). (**C**) Myelin exposure of astrocytes for 24 h increases GFAP immunoreactivity. (**D**) Induction of intracellular reactive oxygen species in myelin-exposed astrocytes after 24 h (myelin, green; CellROX, magenta). Scale bars = 15 μm.

continued to increase for at least 9 days as shown by western blot (Fig. 5B and C). Furthermore, myelin phagocytosis resulted in elevated levels of intracellular reactive oxidative species after 24 h as shown by live cell imaging with a fluorescent probe for oxidative stress (Fig. 5D). Quantification with densitometric analysis of fluorescence intensity showed a 3-fold increase in reactive oxidative species generation [$mean_{untreated} = 1753 \pm 416$, $mean_{myelin\text{-}treated} = 5309 \pm 1409$; one-way ANOVA, $F(1,16) = 29.8$, $P < 0.0001$].

We further examined intracellular astroglial signalling pathways by determining activation of NF-κB and mitogen-activated protein (MAP) kinase p38, a downstream target of LRP1. Myelin uptake by astroglia resulted in nuclear translocation of p65 NF-κB, transient phosphorylation of astroglial p65 NF-κB and degradation of IκBα, suggesting induction of NF-κB signalling (Fig. 6A–C). Astroglial nuclear translocation of p65 NF-κB after incubation with myelin debris was also observed in astrocyte-microglia co-cultures (data not shown). Similarly, p38 MAP kinase signalling was increased in astrocytes after myelin uptake, as indicated by p38 MAPK phosphorylation (Fig. 6D and E). Inhibition of myelin endocytosis through pretreatment with the dynamin inhibitor, Dynasore (0.1 μM, 30 min), reduced IκBα degradation and p38 MAPK phosphorylation, suggesting that myelin uptake rather than LRP1 binding induced both signalling pathways (Fig. 6C and D).

Myelin uptake induces astroglial chemokine production

To determine the effect of myelin phagocytosis on possible immune functions of astrocytes, we analysed mRNA expression and secretion of chemokines, as well as recruitment of T cells and microglia. Expression of 84 immune-relevant genes in untreated and myelin-treated astrocytes were quantified with a PCR array (Supplementary Fig. 4). The genes that were expressed 3.5-fold or higher from baseline are listed in Supplementary Fig. 5A, and are visualized in a scatter plot (Fig. 7A). Of the 17 highly expressed genes, 65% (11) encoded for chemokines, highlighted in red in the scatter plot. Other highly upregulated transcripts included *Nos2*, encoding for inducible nitric oxide synthase (iNOS), and the interleukins *Il1a* (IL-1α) and *Il1b* (IL-1β) (Fig. 7A).

To confirm that transcriptional upregulation resulted in increased production of chemokines, we examined supernatant of cultured astrocytes 24 h after myelin treatment using a cytokine profiler ELISPOT array (Fig. 7B). Myelin exposure induced *de novo* secretion of chemokines (CCL3, CCL5 and CXCL9) and significantly upregulated others (CXCL2, CXCL3, CXCL5, CXCL10 and CCL20). Importantly, interleukins were not detected suggesting that myelin-uptake induced a specific astroglial activation pattern that predominantly supports recruitment of immune cells (Supplementary Fig. 5B).

Finally, to confirm that astroglial chemokine secretion was effective in recruiting immune cells, we analysed migration of polarized T_h1 $CD4^+$ T cells and microglia through a transwell-chamber with conditioned medium from astrocytes in the lower chamber. Conditioned medium from astrocytes treated with myelin increased T_h1 $CD4^+$ cell and microglial migration by 3-fold and 1.6-fold, respectively (Fig. 7C). These data underscore the ability of myelin-stimulated astrocytes to recruit inflammatory cells. Furthermore, we observed that supernatant from myelin-treated astrocytes led to microglial activation *in vitro*, as indicated by their morphological change from

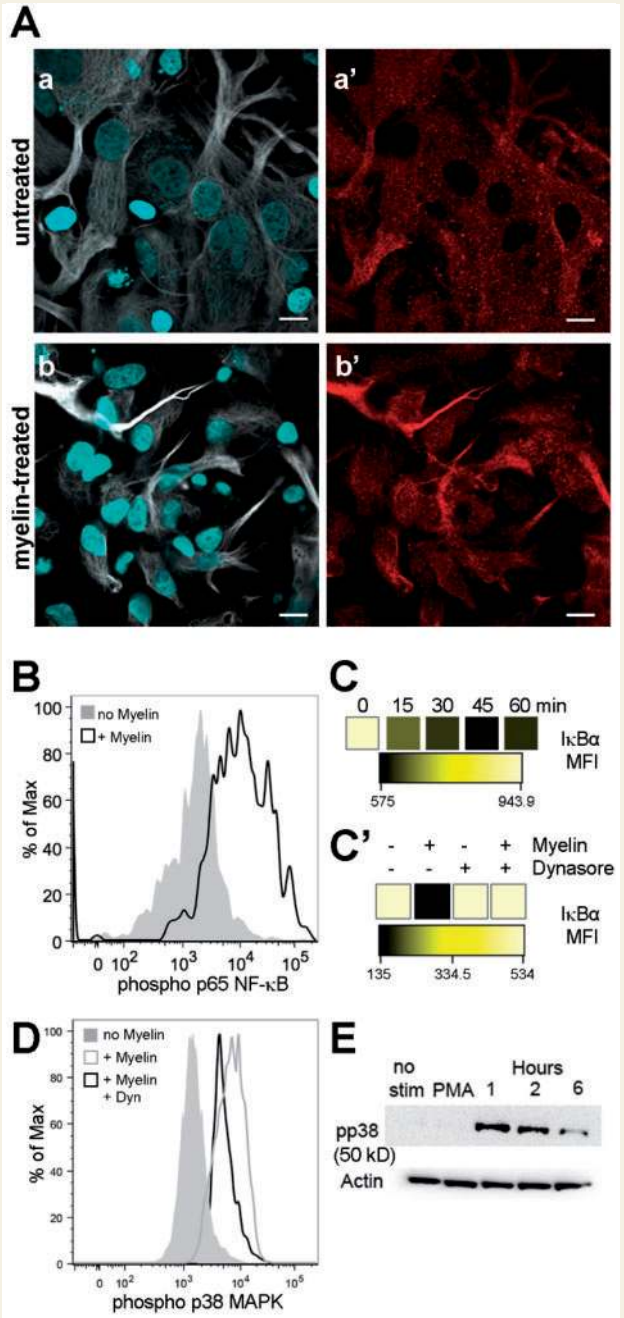

Figure 6 NF-κB and p38 MAP kinase activation in cultured astrocytes exposed to purified myelin. (**A**) Nuclear translocation (Hoechst dye 33342, cyan) of the NF-κB subunit p65 (a' and b', red) after 2 h of exposure with myelin debris (b and b') in GFAP-labelled astrocytes (a and b, grey). (**B**) astroglial p65 phosphorylation (flow cytometry); (**C**) time course (0–60 min) of IκBα degradation with maximum after 45 min of myelin exposure (flow cytometry). (**C'**) Blockade of IκBα degradation after 45 min of myelin exposure by pretreatment with Dynasore (0.1 μM in 1:500 DMSO, 30 min). (**D**) Increased phosphorylation of p38 MAPK after stimulation with myelin for 45 min and partial block after pretreatment with Dynasore (open black; 0.1 μM in 1:500 DMSO, 30 min; flow cytometry). DMSO (1:500) alone has no effect on IκBα degradation or p38 phosphorylation (data not shown). (**B–D**) Representative graphs and heat maps from three independent experiments are shown. (**E**) Transient increase in p38 MAPK phosphorylation after myelin exposure demonstrated by western blot. Scale bars = 15μm in **A**.

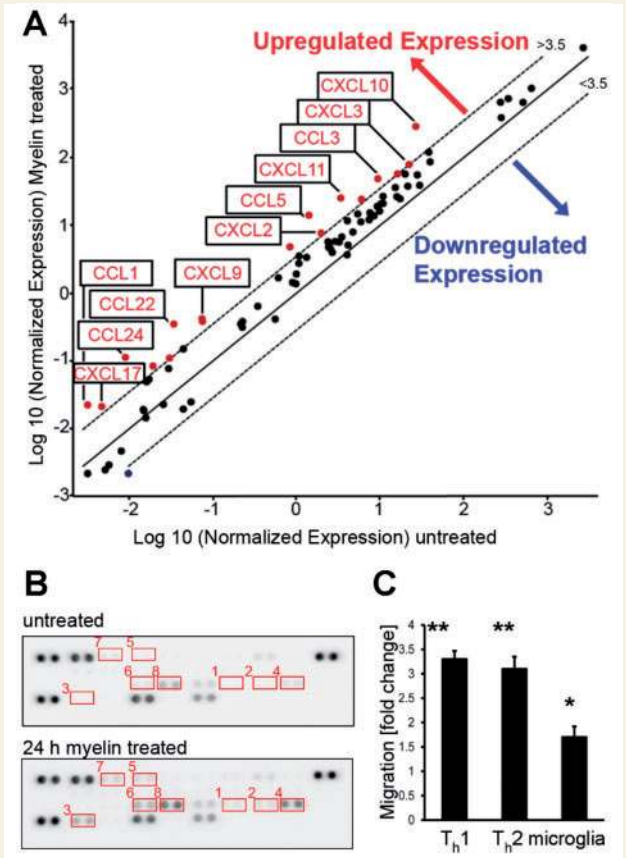

Figure 7 Induction of chemokines in astrocytes through myelin uptake. (**A**) Scatter plot profiling astroglial expression of 84 immune-related genes after incubation with myelin (4 μg/ml; 4 h exposure). Red dots indicate cytokines with a ⩾3.5-fold increase in expression over baseline. (**B**) Representative ELISPOT protein arrays from three independent experiments showing induced and upregulated cytokine expression in astroglial supernatant (red squares: 1 = CCL5, 2 = CXCL9, 3 = CCL3, 4 = CCL20, 5 = CXCL2, 6 = CXCL10, 7 = CXCL3, 8 = CXCL5). (**C**) Directed migration of polarized $CD4^+$ T_h1 and microglia in conditioned medium from myelin-treated astrocytes (2 μg/ml for 24 h) in trans-well-chambers. Data represent the means ± SD from three independent experiments [one-way ANOVA, $F(3,8) = 26.08$, $P < 0.001$; Tukey–Kramer test, $^*P < 0.05$, $^{**}P < 0.01$].

an elongated and bipolar to a rounded shape with short processes (Supplementary Fig. 6).

Quantification of chemokines and iNOS expression, and NF-κB nuclear localization in areas of myelin breakdown

To verify the relevance of our *in vitro* findings in human disease, we quantified the expression of selected chemokines that were upregulated in astrocytes after myelin uptake *in vitro* (CCL3, CCL5, CCL20 and CXCL10) in myelin-laden hypertrophic astrocytes, myelin-negative reactive astrocytes and myelin-laden macrophages in areas of active demyelination. In addition, we examined

expression of iNOS and nuclear translocation of p65 NF-κB in these cells.

Our data indicate that expression of chemokines was overall significantly higher in myelin-laden astrocytes compared to that in myelin-negative astrocytes in multiple sclerosis, progressive multifocal leukoencephalopathy and subacute ischaemic infarct (Fig. 8 and Supplementary Fig. 7). Similarly, we found increased nuclear localization of p65 NF-κB in hypertrophic myelin-laden astrocytes compared to myelin-negative astrocytes. In contrast, iNOS expression was highly variable but not significantly different between myelin-positive and myelin-negative astrocytes and myelin-laden macrophages. Of note, chemokines were expressed at low levels in hypertrophic but myelin-negative astrocytes in progressive multifocal leukoencephalopathy, comparable to myelin-negative reactive astrocytes. The chemokine profile differed between different diseases: in multiple sclerosis, expression of CXCL10 was highest, followed by CCL5, CCL3 and CCL20 by myelin-positive astrocytes, whereas myelin-laden macrophages showed high immunoreactivity for CCL20 and CCL3. In cerebral infarct, chemokine expression was overall lower with CCL20 being most highly expressed by hypertrophic astrocytes. In progressive multifocal leukoencephalopathy, CXCL10 and CCL3 were highly expressed by hypertrophic astrocytes, but not in macrophages, while CCL5 and CCL20 were moderately expressed by both hypertrophic astrocytes and macrophages.

Discussion

Here we report that the vast majority of astrocytes in areas of active myelin breakdown contained myelin debris in multiple sclerosis, progressive multifocal leukoencephalopathy, metachromatic leukodystrophy and subacute cerebral infarcts. These myelin-positive astrocytes were concentrated at the advancing edge of myelin damage and were invariably hypertrophic but contained substantially less myelin than myelin-laden macrophages. The presence of myelin-containing, hypertrophic astrocytes extended into adjacent normal-appearing white matter, which is characterized by scattered activated microglia but not myelin-laden macrophages. This spatial distribution suggests that myelin

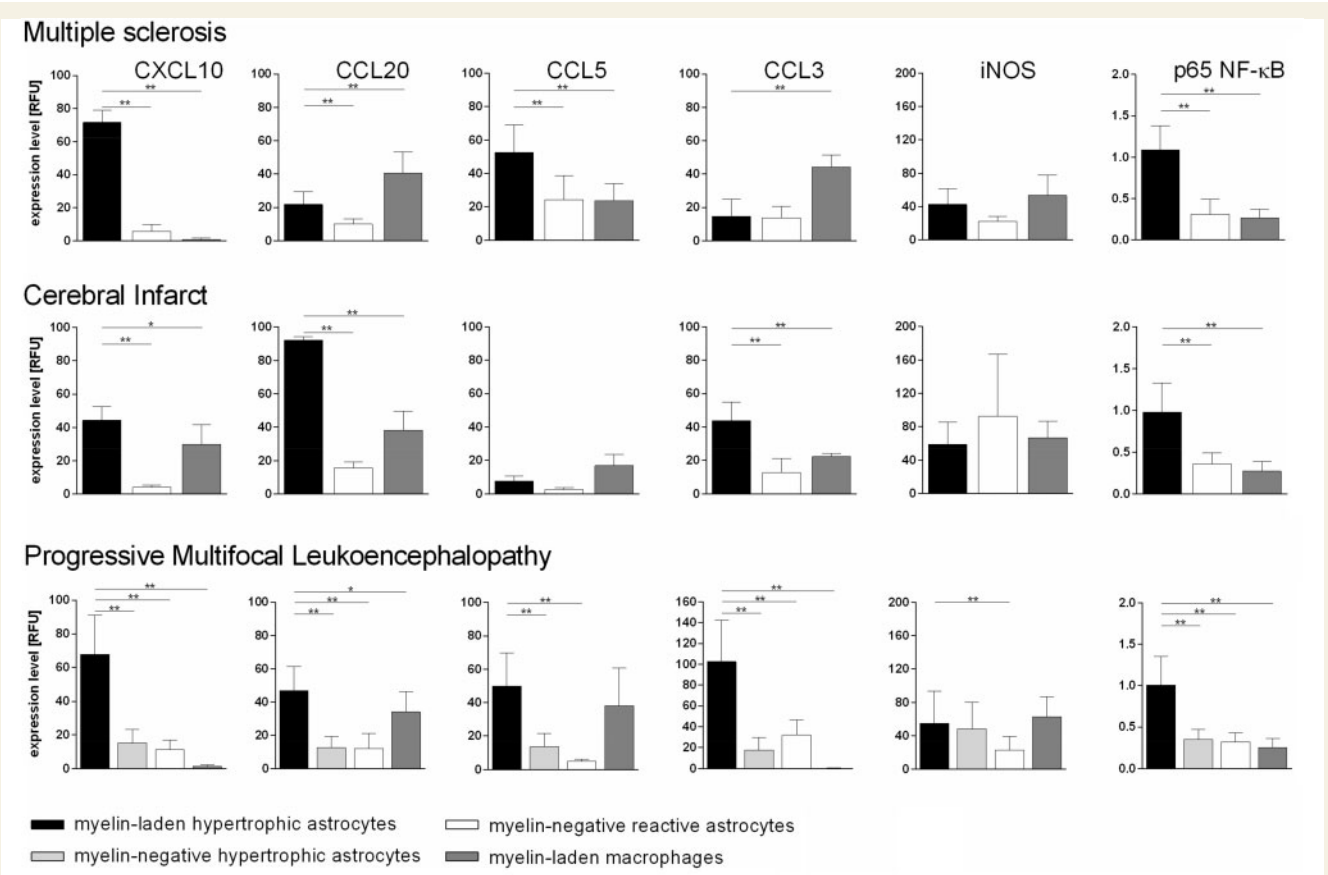

Figure 8 Quantification of chemokines and iNOS expression, and NF-κB nuclear localization in areas of myelin breakdown. Graphs display fluorescent immunoreactivity means ± SD of CXCL10, CCL20, CCL3, CCL5, iNOS and nuclear localization of p65 NF-κB in myelin-positive hypertrophic astrocytes, myelin-negative reactive astrocytes and myelin-laden macrophages, quantified by densitometric analysis. For statistical analysis one-way ANOVA with Tukey-Kramer test for individual comparisons from at least 20 cells per cell type per case was performed. *$P < 0.05$, **$P < 0.01$.

uptake by astrocytes is an early event that occurs before the bulk of damaged myelin is cleared by macrophages.

In cell culture, myelin-uptake by astrocytes induced NF-κB and MAP kinase activation as well secretion of lymphocyte- and macrophage-attracting chemokines. Consistent with these *in vitro* results, we observed in the human diseases that myelin-containing astrocytes displayed increased NF-κB activation and expressed substantially higher chemokine levels (CCL3, CCL5, CCL20 and CXCL10) compared to reactive, myelin-negative astrocytes. Our results suggest that myelin phagocytosis is a universal astroglial response in CNS diseases with prominent myelin injury. Furthermore, while astrocytes do not contribute significantly to myelin removal compared to professional phagocytes, they may initiate a first line response to myelin injury that leads to recruitment of immune cells to the lesion site.

Our findings in post-mortem tissue are in line with two previous studies that examined CNS tissue from patients with relapsing-remitting and primary progressive multiple sclerosis (Lee *et al.*, 1990; Morcos *et al.*, 2003). In both studies, myelin fragments were found in hypertrophic astrocytes in early and chronic active lesions as well as in remyelinating lesions (Morcos *et al.*, 2003), a lesion type that we did not examine. Intriguingly, Lee *et al.* (1990) described processes of myelin-phagocytosing astrocytes that were interpositioned between axons and their disrupted myelin sheaths, suggesting that astrocytes directly remove damaged myelin from axons. To our knowledge, myelin particles in astroglia have been reported in multiple sclerosis but not in any of the other human demyelinating conditions examined here. Several animal studies have demonstrated that astrocytes are capable of phagocytosis: astrocytes have been shown to phagocytose synapses in the developing and adult mouse CNS (Chung *et al.*, 2013) and axonal and myelin debris in animal models of entorhinal cortex (Bechmann and Nitsch, 2000), optic nerve injury (Colavincenzo and Levine, 2000) and in *ex vivo* tissue cultures exposed to EAE serum (Raine and Bornstein, 1970).

We furthermore established that myelin debris was taken up by astrocytes via the scavenger receptor low density LRP1 and entered the endosomal-lysosomal degradative pathway. LRP1 is a multifunctional and promiscuous membrane receptor that binds to over 40 distinct ligands (Gonias and Campana, 2014). LRP1 has been shown to facilitate astroglial endocytosis of tissue plasminogen activator and amyloid-β (Casse *et al.*, 2012; Birch, 2014) and is upregulated in reactive astrocytes in and around areas of active demyelination in multiple sclerosis (Hendrickx *et al.*, 2013), after ischaemic injury (Zhang *et al.*, 2007) and in Schwann cells after peripheral nerve injury (Campana *et al.*, 2006). Here we report that LRP1 was highly expressed both in myelin debris-positive astrocytes and macrophages *in vivo*, consistent with the report that LRP1 is essential for myelin phagocytosis by macrophages (Gaultier *et al.*, 2009). This selective upregulation of LRP1 in tissue contrasts with the constitutive expression that we observed in cultured astroglia irrespective of their activation status.

In macrophages, myelin phagocytosis induces an anti-inflammatory (M2) phenotype that is thought to limit and eventually resolve lesional inflammation in multiple sclerosis (Boven *et al.*, 2006), consistent with the anti-inflammatory effects of LRP1 signalling in macrophages (Gonias and Campana, 2014). In contrast, myelin uptake by astrocytes does not induce expression of pro- or anti-inflammatory cytokines; therefore, expression of chemokines occurs in the absence of astroglial polarization.

We hypothesize that myelin-containing astrocytes exert a major effect on lesion development through chemoattraction of immune cells. This may lead to increased tissue damage in demyelinating conditions driven by inflammation such as multiple sclerosis, where additional recruitment of lymphocytes and microglia/macrophages fuels the inflammatory process. On the other hand, microglia and monocyte recruitment may be beneficial for myelin clearance in a non-inflammatory environment. This is suggested by studies in mice depleted of reactive astrocytes, where treatment with the oligodendrocyte toxin cuprizone led to reduced microglial recruitment with concomitant failure of removal of myelin debris and delay in remyelination (Skripuletz *et al.*, 2013). In addition, reactive astrocytes fulfil a number of neurosupportive and homeostatic functions that may be altered by myelin uptake; however, this has not been examined in our study. Finally, although astrocytes express chemokines in all conditions examined (multiple sclerosis, progressive multifocal leukoencephalopathy and cerebral infarct), substantial lymphocyte infiltrates are typically not seen in cerebral infarcts or metachromatic leukodystrophy. Thus, other factors such as peripheral lymphocyte activation and blood–brain barrier permeability may ultimately determine the degree of lymphocyte infiltration.

In summary, our findings suggest that astroglial phagocytosis of myelin debris is common in CNS pathologies with prominent myelin injury. While it is impossible to determine the exact chronological sequence with histological samples, it is possible that myelin uptake by astrocytes is an early response to myelin damage and may trigger pro-inflammatory activation injury. Moreover, myelin uptake induces a specific astroglial phenotype associated with secretion of cell-recruiting chemokines that leads to influx of immune cells and to the bulk removal of damaged myelin by macrophages. Thus, modulation of early astroglial responses to myelin damage may be of considerable therapeutic import to prevent subsequent inflammation in multiple sclerosis and other diseases with prominent myelin injury. Indeed, several treatments for multiple sclerosis, fingolimod, dimethyl fumarate and laquinimod have been shown to directly inhibit astrocytic activation (Wilms *et al.*, 2010; Choi *et al.*, 2011; Bruck *et al.*, 2012), which is likely to contribute to their overall therapeutic effect.

Acknowledgements

We would like to acknowledge the Rocky Mountain Multiple Sclerosis Center Tissue Bank for providing some of the post-mortem brain tissue used in this study.

Funding

This study was supported by grants from the National Multiple Sclerosis Society to the PI (PP1796) and to the Rocky Mountain Multiple Sclerosis Center Tissue Bank. This publication was also made possible by CTSA Grant UL1 RR024139 from the National Center for Advancing Translational Science (NCATS), a component of the National Institutes of Health (NIH), and NIH roadmap for Medical Research. Its contents are solely the responsibility of the authors and do not necessarily represent the official view of NIH.

Supplementary material

Supplementary material is available at *Brain* online.

References

Bechmann I, Nitsch R. Involvement of non-neuronal cells in entorhinal-hippocampal reorganization following lesions. Ann N Y Acad Sci 2000; 911: 192–206.

Birch AM. The contribution of astrocytes to Alzheimer's disease. Biochem Soc Trans 2014; 42: 1316–20.

Boster AL, Nicholas JA, Topalli I, Kisanuki YY, Pei W, Morgan-Followell B, et al. Lessons learned from fatal progressive multifocal leukoencephalopathy in a patient with multiple sclerosis treated with natalizumab. JAMA Neurol 2013; 70: 398–402.

Boven LA, Van Meurs M, Van Zwam M, Wierenga-Wolf A, Hintzen RQ, Boot RG, et al. Myelin-laden macrophages are anti-inflammatory, consistent with foam cells in multiple sclerosis. Brain 2006; 129 (Pt 2): 517–26.

Brosnan CF, Raine CS. The astrocyte in multiple sclerosis revisited. Glia 2013; 61: 453–65.

Bruck W, Pfortner R, Pham T, Zhang J, Hayardeny L, Piryatinsky V, et al. Reduced astrocytic NF-kappaB activation by laquinimod protects from cuprizone-induced demyelination. Acta Neuropathol 2012; 124: 411–24.

Campana WM, Li X, Dragojlovic N, Janes J, Gaultier A, Gonias SL. The low-density lipoprotein receptor-related protein is a pro-survival receptor in Schwann cells: possible implications in peripheral nerve injury. J Neurosci 2006; 26: 11197–207.

Casse F, Bardou I, Danglot L, Briens A, Montagne A, Parcq J, et al. Glutamate controls tPA recycling by astrocytes, which in turn influences glutamatergic signals. J Neurosci 2012; 32: 5186–99.

Choi JW, Gardell SE, Herr DR, Rivera R, Lee CW, Noguchi K, et al. FTY720 (fingolimod) efficacy in an animal model of multiple sclerosis requires astrocyte sphingosine 1-phosphate receptor 1 (S1P1) modulation. Proc Natl Acad Sci USA 2011; 108: 751–6.

Chung WS, Clarke LE, Wang GX, Stafford BK, Sher A, Chakraborty C, et al. Astrocytes mediate synapse elimination through MEGF10 and MERTK pathways. Nature 2013; 504: 394–400.

Colavincenzo J, Levine RL. Myelin debris clearance during Wallerian degeneration in the goldfish visual system. J Neurosci Res 2000; 59: 47–62.

Costales P, Castellano J, Revuelta-Lopez E, Cal R, Aledo R, Llampayas O, et al. Lipopolysaccharide downregulates CD91/low-density lipoprotein receptor-related protein 1 expression through SREBP-1 overexpression in human macrophages. Atherosclerosis 2013; 227: 79–88.

Croitoru-Lamoury J, Guillemin GJ, Boussin FD, Mognetti B, Gigout LI, Cheret A, et al. Expression of chemokines and their receptors in human and simian astrocytes: evidence for a central role of TNF alpha and IFN gamma in CXCR4 and CCR5 modulation. Glia 2003; 41: 354–70.

D'Amelio FE, Smith ME, Eng LF. Sequence of tissue responses in the early stages of experimental allergic encephalomyelitis (EAE): immunohistochemical, light microscopic, and ultrastructural observations in the spinal cord. Glia 1990; 3: 229–40.

Gaultier A, Wu X, Le Moan N, Takimoto S, Mukandala G, Akassoglou K, et al. Low-density lipoprotein receptor-related protein 1 is an essential receptor for myelin phagocytosis. J Cell Sci 2009; 122 (Pt 8): 1155–62.

Gieselmann V, Krageloh-Mann I. Metachromatic leukodystrophy–an update. Neuropediatrics 2010; 41: 1–6.

Gonias SL, Campana WM. LDL receptor-related protein-1: a regulator of inflammation in atherosclerosis, cancer, and injury to the nervous system. Am J Pathol 2014; 184: 18–27.

Greenfield JG, Love S, Louis DN, Ellison D. Greenfield's neuropathology. 8th ed. London: Hodder Arnold; 2008. pp. 198–9; 535–9; 1340–2.

Hendrickx DA, Koning N, Schuurman KG, van Strien ME, van Eden CG, Hamann J, et al. Selective upregulation of scavenger receptors in and around demyelinating areas in multiple sclerosis. J Neuropathol Exp Neurol 2013; 72: 106–18.

Housley WJ, Adams CO, Vang AG, Brocke S, Nichols FC, LaCombe M, et al. Peroxisome proliferator-activated receptor gamma is required for CD4+ T cell-mediated lymphopenia-associated autoimmunity. J Immunol 2011; 187: 4161–9.

Lassmann H, Brück W, Lucchinetti C. The immunopathology of multiple sclerosis: an overview. Brain Pathol 2007; 17: 210–8.

Lee SC, Moore GR, Golenwsky G, Raine CS. Multiple sclerosis: a role for astroglia in active demyelination suggested by class II MHC expression and ultrastructural study. J Neuropathol Exp Neurol 1990; 49: 122–36.

McCarthy KD, de Vellis J. Preparation of separate astroglial and oligodendroglial cell cultures from rat cerebral tissue. J Cell Biol 1980; 85: 890–902.

Mehlem A, Hagberg CE, Muhl L, Eriksson U, Falkevall A. Imaging of neutral lipids by oil red O for analyzing the metabolic status in health and disease. Nat Protoc 2013; 8: 1149–54.

Morcos Y, Lee SM, Levin MC. A role for hypertrophic astrocytes and astrocyte precursors in a case of rapidly progressive multiple sclerosis. Mult Scler 2003; 9: 332–41.

Norton WT, Poduslo SE. Myelination in rat brain: method of myelin isolation. J Neurochem 1973; 21: 749–57.

Nylander A, Hafler DA. Multiple sclerosis. J Clin Invest 2012; 122: 1180–8.

Pham H, Ramp AA, Klonis N, Ng SW, Klopstein A, Ayers MM, et al. The astrocytic response in early experimental autoimmune encephalomyelitis occurs across both the grey and white matter compartments. J Neuroimmunol 2009; 208: 30–9.

Pitt D, Nagelmeier IE, Wilson HC, Raine CS. Glutamate uptake by oligodendrocytes: implications for excitotoxicity in multiple sclerosis. Neurology 2003; 61: 1113–20.

Ponath G, Schettler C, Kaestner F, Voigt B, Wentker D, Arolt V, et al. Autocrine S100B effects on astrocytes are mediated via RAGE. J Neuroimmunol 2007; 184: 214–22.

Raine CS, Bornstein MB. Experimental allergic encephalomyelitis: an ultrastructural study of experimental demyelination in vitro. J Neuropathol Exp Neurol 1970; 29: 177–91.

Schneider CA, Rasband WS, Eliceiri KW. NIH Image to ImageJ: 25 years of image analysis. Nat Methods 2012; 9: 671–5.

Skripuletz T, Hackstette D, Bauer K, Gudi V, Pul R, Voss E, et al. Astrocytes regulate myelin clearance through recruitment of microglia during cuprizone-induced demyelination. Brain 2013; 136 (Pt 1): 147–67.

Wang D, Ayers MM, Catmull DV, Hazelwood LJ, Bernard CC, Orian JM. Astrocyte-associated axonal damage in pre-onset stages of experimental autoimmune encephalomyelitis. Glia 2005; 51: 235–40.

Werner P, Pitt D, Raine CS. Multiple sclerosis: altered glutamate homeostasis in lesions correlates with oligodendrocyte and axonal damage. Ann Neurol 2001; 50: 169–80.

Wilms H, Sievers J, Rickert U, Rostami-Yazdi M, Mrowietz U, Lucius R. Dimethylfumarate inhibits microglial and astrocytic inflammation by suppressing the synthesis of nitric oxide, IL-1beta, TNF-alpha and IL-6 in an in-vitro model of brain inflammation. J Neuroinflammation 2010; 7: 30.

Yu Z, Yu P, Chen H, Geller HM. Targeted inhibition of KCa3.1 attenuates TGF-beta-induced reactive astrogliosis through the Smad2/3 signaling pathway. J Neurochem 2014; 130: 41–9.

Zhang X, Polavarapu R, She H, Mao Z, Yepes M. Tissue-type plasminogen activator and the low-density lipoprotein receptor-related protein mediate cerebral ischemia-induced nuclear factor-kappaB pathway activation. Am J Pathol 2007; 171: 1281–90.